ELSEVIER

Surface Science 365 (1996) 591–601

surface science

Growth and structure of Pd alloys on Cu(100)

P.W. Murray *, I. Stensgaard, E. Lægsgaard, F. Besenbacher

Center for Atomic-scale Materials Physics, and Institute of Physics and Astronomy, University of Aarhus, DK 8000 Aarhus C, Denmark

Received 23 February 1996; accepted for publication 18 April 1996

Abstract

The growth and structure of Pd alloys formed on Cu(100) have been studied from the initial nucleation to the formation of a second-layer structure, using scanning tunneling microscopy (STM) and Rutherford backscattering spectroscopy (RBS). The STM images show that individual Pd atoms initially alloy into lattice sites of the substrate, with a preference for occupation of second-nearest neighbor (NN) sites. This results in the formation of short, [001] and [010]-directed chains of Pd atoms which converge to form a $c(2\times2)$ structure as the coverage is increased. Copper atoms ejected by the incorporation of Pd into the surface form Cu islands on the terraces. The growth of such islands on the alloyed terraces results in subsurface Pd, and consequently, a greater amount of Pd is required to form the $c(2\times2)$ structure than the ideal 0.5 monolayer (ML). Nucleation of the second Pd layer is seen at upper step edges before the first layer $c(2\times2)$ structure is completed. Continued deposition of Pd results in completion of the $c(2\times2)$ structure and further growth of the second (topmost) layer phase which from LEED appears to have a p4g symmetry, while a $p(2\times2)$ periodicity is revealed by STM. A model is proposed in which the second layer is a mixed alloy layer of Pd and Cu forming on top of a p4g reconstructed $c(2\times2)$ first layer.

Keywords: Alloys; Copper; Growth; Palladium; Scanning tunneling microscopy; Surface structure

1. Introduction

Recently, there has been considerable interest in metal-on-metal growth from both a fundamental point of view and the technological relevance of novel chemical, electronic and magnetic properties of thin metal films. The use of scanning tunneling microscopy (STM) has given a great insight into such systems and has shown that in many cases, the structures formed have been much more complicated than originally anticipated, with many variations to the three standard growth modes [1]. In particular, many systems have been shown to exhibit surface-alloy formation in which the deposited metal intermixes with the topmost layer of the substrate rather than forming a simple overlayer structure [2]. Such alloys have even been observed between metals which are immiscible in the bulk [3–6]. Information regarding the intermixing and alloy formation is important in understanding the properties of such structures, but little detailed information concerning the initial stages of alloy formation at the atomic level is available.

On the Cu(100) surface, a number of metal adsorbates such as Pb [6], Au [7], Mn [8–10] and Pd [11–14] are known to form a surface alloy with a $c(2\times2)$ structure at a coverage of approximately 0.5 ML. The Pd-alloy structures on Cu(100) have been the subject of a number of investigations due to their relevance as bimetallic catalysts in

* Corresponding author. Fax: +45 8612 0740; e-mail: pwm@dfi.aau.dk

PII S0039-6028(96)00748-0

applications such as methanol synthesis [15] and acetylene hydrogenation [16]. Studies have also demonstrated modified adsorption properties of CO on the Pd/Cu(100) system [17]. The formation of a surface alloy on the Pd/Cu(100) system was first confirmed in a low energy electron diffraction (LEED) analysis of a Pd-induced c(2 × 2) structure, which ruled out the formation of an ordered c(2 × 2) ovelayer in favor of a surface alloy [11]. Further support for the alloy formation was derived from photo-emission studies in which Pd features similar to those seen for Cu rich bulk CuPd alloys were observed [11]. The surface-alloy model has also been supported by local density approximation (LDA) calculations [18]. However, the structures are not as simple as one might expect. For example, no consensus has been reached for the Pd coverage corresponding to the optimum c(2 × 2) structure, as judged from the LEED intensity of the half-order beams. Graham and coworkers [12,17] have reported an optimal coverage of 0.8 ML while Wu et al. [11] and Pope et al. [13] reported that ≈0.5 ML was the best coverage. Furthermore, the existence of Pd below the surface layer has been evidenced based on different techniques. Low energy ion scattering (LEIS) studies [12] suggested incorporation of Pd beyond the surface since the Cu signal decayed only to 70% upon formation of the c(2 × 2) structure, compared to the expected 50%. By using CO as a probe molecule for a Pd coverage of 0.5 ML, Valden et al. [19] reported that approximately 40% of the outer layer was pure (non-alloyed) Cu, with the excess Pd located below the surface. More recently, medium energy ion scattering (MEIS) studies have indicated that at 0.5 ML Pd coverage, the c(2 × 2) structure is incomplete due to subsurface Pd [20].

Continued deposition beyond the c(2 × 2) phase results in the formation of a p(2 × 2)p4g second-layer structure [20]. Structural studies of this phase (MEIS, LEED) have given evidence that the second-layer structure formed at approximately 1 ML is a mixed structure consisting of both Pd and Cu [20,22]. However, structural models for this phase, which are entirely consistent with these data, have not been established due to the complexity of the alloy formation and growth.

In this paper, we report in full (using STM and Rutherford backscattering spectroscopy (RBS)), the growth and structure of Pd alloys on Cu(100) at room temperature (RT), starting with the initial nucleation and growth, proceeding through the formation of the c(2 × 2) alloy and finally going to the (2 × 2)p4g second-layer phase. This follows our preliminary report of the initial stages leading up to the c(2 × 2) structure [23]. The results show how the initial nucleation of the alloy occurs and elucidates the formation of the c(2 × 2) structure as the coverage increases. The mechanism by which Pd goes subsurface is revealed, together with an explanation behind the reported discrepancy in Pd coverage required to form the c(2 × 2) structure. In addition, results on the second-layer growth show that this phase is initially nucleated at upper-step and island edges. STM images show a p(2 × 2) periodicity for the terminating layer rather than a p4g structure. A model is proposed which consists of a mixed p(2 × 2) top layer above a clock rotated c(2 × 2) structure.

2. Experimental

These experiments were performed using a fully automated STM [24] operated at RT. The STM was mounted in an ultrahigh vacuum (UHV) chamber (base pressure 1×10^{-10} mbar), interfaced to a 2 MV van de Graaff accelerator via differential pumping, and containing standard facilities for sample cleaning and characterization. The Cu(100) crystal was prepared by repeated cycles of Ne-ion bombardment (3 keV) and annealing (770 K) until judged clean and well ordered by Auger electron spectroscopy (AES), LEED and STM. Typical atomic-resolution and large-scale images of the clean Cu(100) surface, which show large flat terraces, are displayed in Fig. 1. Pd evaporation was carried out by resistively heating a conical tungsten filament containing a Pd wire, and the absolute Pd coverage calibrations were obtained by RBS [25]. Palladium deposition was carried out with the sample at RT, after allowing the source to stabilize prior to exposure of the sample. The pressure during deposition was below 1×10^{-9} mbar. Deposition rates were on the order of 0.2

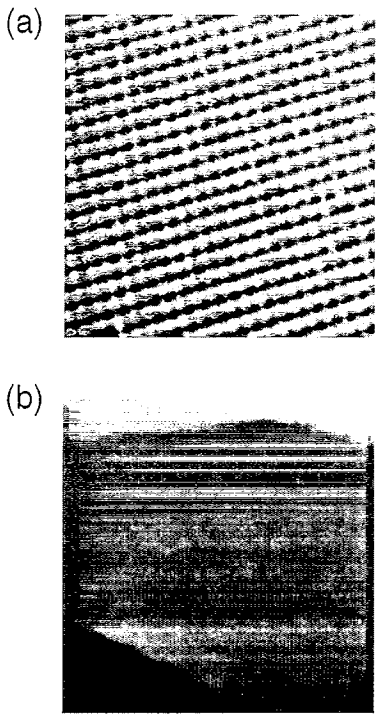

Fig. 1. (a) STM image (50×50 Å^2) of the clean Cu(100) surface prior to Pd deposition, showing atomic resolution. (b) Large-scale image (1000×1000 Å^2), showing large flat terraces and smooth step edges.

ML min^{-1}, with 1 ML defined as the Cu(100) surface-atom density (1.53×10^{15} atoms cm^{-2}). STM images were recorded in the constant current mode, with typical tunneling parameters of 2 nA current and -10 mV sample bias. Changes in polarity had no significant effect on the images.

3. Results and discussion

3.1. Initial alloy formation

An STM image recorded after deposition of 0.20 ML, as determined by RBS, is shown in Fig. 2a in which a number of protrusions can be observed on the image. The number of these protrusions increases with continued Pd deposition. From a (1×1) unit mesh superimposed on the image, it can be seen that the protrusions are located directly on Cu sites in the surface and not in fourfold hollow sites. The height of these features varies from 0.1 to 0.3 Å, depending on such factors as tunneling parameters and tip quality with corrugation heights on the Cu(100) surface being on the order of 0.1 Å. During repeated scans over the same area, no evidence was observed for any diffusion of the protrusions, indicating their stability in the Cu substrate at RT. Occasionally, after a tip change, they can be imaged as depressions, as illustrated in Fig. 2b, indicating that the contrast is strongly dependent on the chemical identity of the tip.

Fig. 2c shows that together with the formation of protrusions, there is island formation on the terraces, in contrast to the smooth terraces shown in Fig. 1. Atomically resolved images of such islands are consistent with a Cu(100)1×1 structure, and the height of the islands is identical to a monatomic step on Cu(100). We therefore attribute the protrusions to Pd atoms alloyed into the surface layer and the islands to Cu atoms ejected from the terraces upon incorporation of Pd atoms to form a surface alloy. A one-to-one correspondence between the deposited Pd and ejected Cu atoms is difficult to verify experimentally due to the fact that it is impossible to identify the amount of Cu that has migrated to steps. In the case of Au alloying on Ni(110) [3], a similar interpretation was given for the islands observed. Although Pd atoms are also observed on the islands, their density is somewhat less than on the terraces, especially at the edges of the islands. The area covered by the islands also increases as a function of Pd coverage, as evidenced in Fig. 2d where the surface has been exposed to 0.4 ML of Pd (RBS). In regions with a high step density, very few islands are seen, suggesting that the ejected Cu atoms diffuse to nearby step edges, which is further supported by the observation that the step edges are more jagged as compared to the smooth step edges on clean Cu(100). For Cu(100) surfaces alloyed with Au and Mn, similar observations of step-edge shapes have been made [7,9].

The Pd coverage, as determined from a number of STM images similar to Fig. 2a, is 0.15 ML, somewhat less than that obtained from RBS (0.20 ML). However, any Pd located beneath the surface would not be detected by STM. Thus we ascribe the discrepancy between the STM and RBS cover-

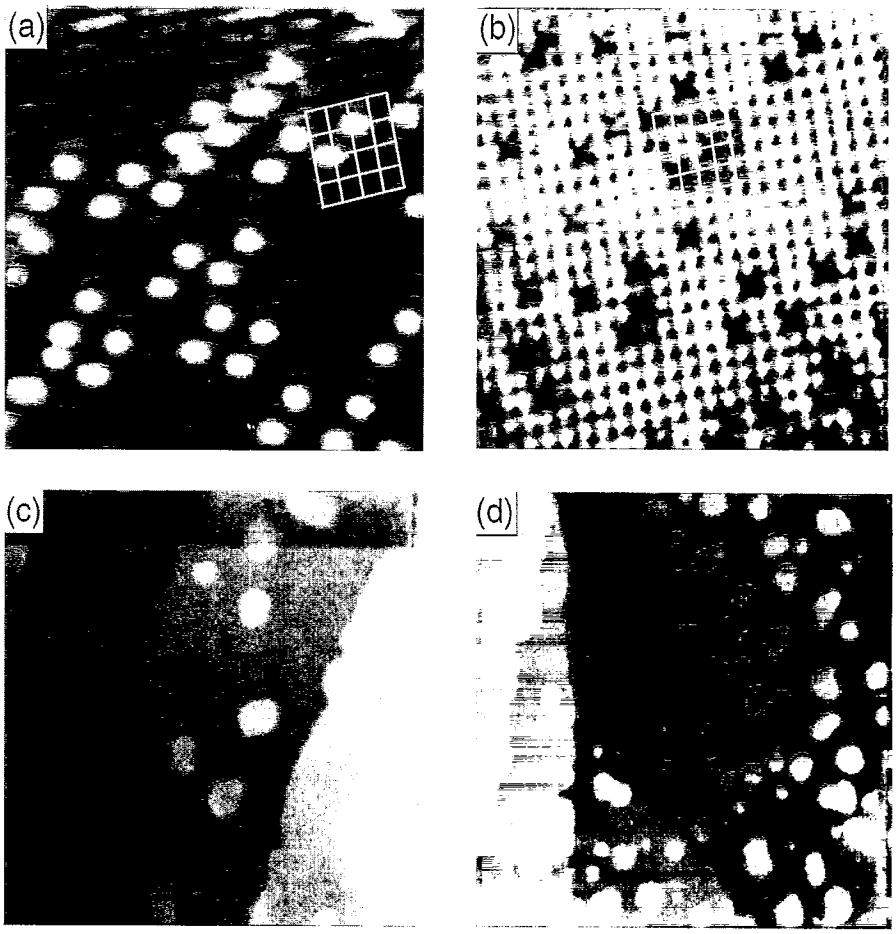

Fig. 2. (a) A 50×50 Å^2 image of Cu(100) following 0.20 ML Pd deposition, showing the appearance of protrusions on the substrate. By superimposing a (1×1) unit mesh, it can be seen that the protrusions are located on lattice sites of the substrate. (b) STM image recorded after a tip change, in which the protrusions are now imaged as depressions (50×50 Å^2). (c) A 1000×1000 Å^2 image recorded after 0.20 ML Pd deposition, showing the formation of islands on the terraces and a roughening of step edges. (d) A 1500×1500 Å^2 image after 0.40 ML Pd deposition, showing the nucleation of smaller islands in between the larger ones.

age determinations to subsurface Pd "buried" by newly formed Cu islands and expanding Cu step edges growing on top of Pd decorated regions. Previous results of the $c(2 \times 2)$ alloy structure have also shown evidence for subsurface Pd [17,19]. STM images reveal that the density of Pd atoms on islands and close to step edges is less than that on the terraces, indicating that Pd located below the islands does not diffuse to the surface. This is not surprising, given that Pd and Cu form stable bulk alloys.

Inspection of images like that in Fig. 2a reveals that the majority of Pd atoms on the terraces appear not to be distributed randomly, but are located in a 2nd NN position to another Pd atom, i.e. in sites preferentially aligned along the [010] and [001] directions. A pair-correlation plot of the NN distribution for Pd atoms out to a distance of 6th NN positions, taken over a number of images with a Pd coverage of 0.20 ML (RBS), is shown in Fig. 3a, which further supports this. The expected occupations based on a perfect random distribution, and a pseudo-random distribution generated for the number of images and Pd atoms used in the data set, are also shown for comparison. A measure of the reliability of the data set are given by the latter; the closer this matches the distribution of genuine random positions, the more

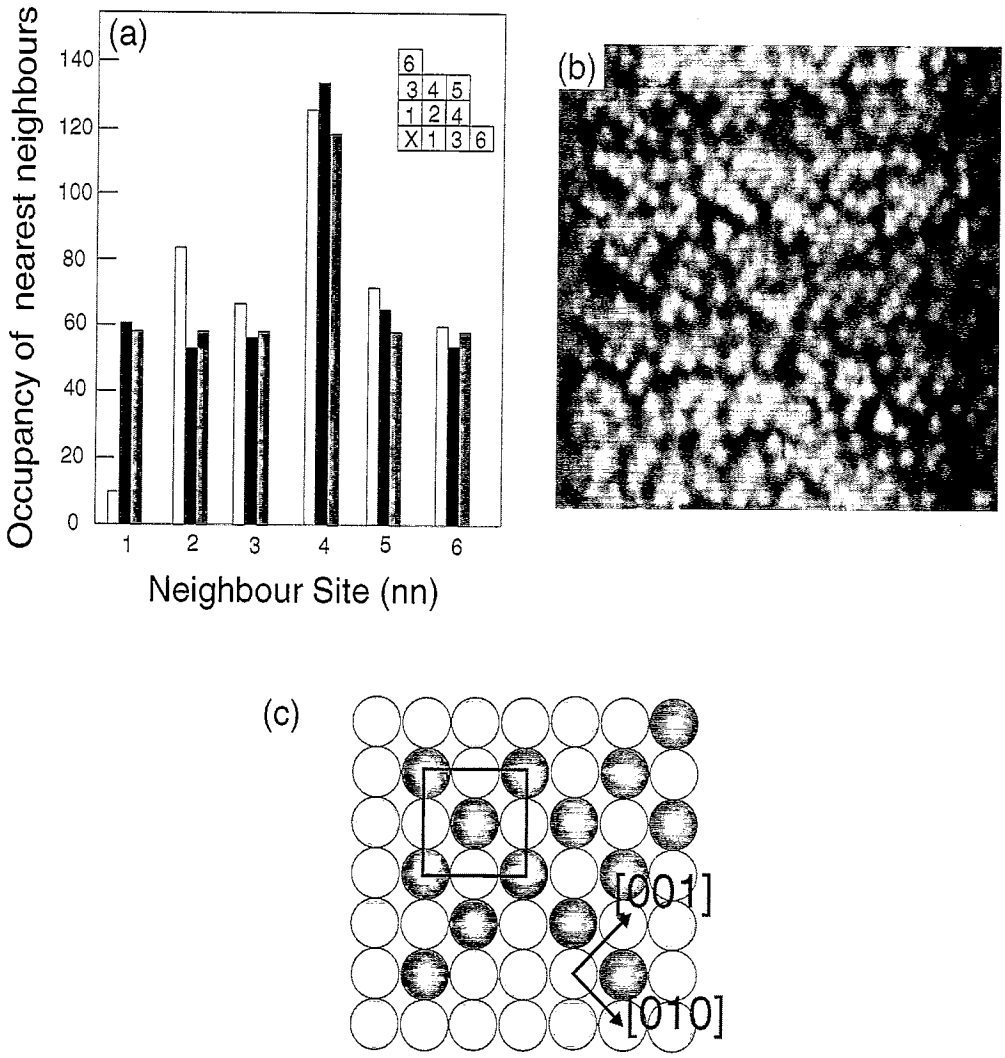

Fig. 3. (a) Histogram of the occupancy of Pd atoms as a function of NN distance up to 6th NN for 96 Pd atoms from a number of images at 0.20 ML coverage (open bars), the expected occupancy for a totally random distribution (shaded bars) and a random simulation on the images from which the data was acquired (filled bars). There are significantly smaller (greater) peaks for the 1st (2nd) NN positions. (b) 100×100 Å^2 image at 0.45 ML Pd, revealing the formation of short rows of Pd atoms along the [001] and [010] directions. Where the chains converge, small $c(2 \times 2)$ domains are formed, as depicted schematically in (c) where lightly (heavily) shaded balls represent Cu (Pd) atoms, respectively.

statistically reliable the data set. The histogram confirms that the distribution is not random, with the number of Pd atoms located in first NN sites being much lower than expected for a random distribution, while there is a significant increase in the occupation of second NN positions, that is, along the [010] and [001] directions. Recent calculations on surface alloying by Tersoff [26] are also consistent with this finding. By taking into account the strain energy caused by atomic mismatch, Tersoff showed that a second NN occupancy is energetically favorable for alloying on metal (100) surfaces. Thus the initial nucleation of the alloy occurs via the formation of chains along [001] and [010] directions, with an elongation of the chains as the coverage increases, as illustrated in Fig. 3b, where the Pd coverage has been increased to 0.35 ML, as determined by RBS. Small

c(2 × 2) units are formed where the perpendicular chains converge, as shown schematically in Fig. 3c. The coverage determined from a number of STM images (0.29 ML) is again lower than that obtained from RBS (0.35 ML), which is again attributed to subsurface Pd located beneath islands and expanding steps.

The Cu-island size and distribution reveal that at low Pd coverages (≈0.2 ML), islands are formed at typical separations of 150 to 200 Å, indicating that the diffusion length of the Cu atoms on the alloyed surface is on the order of 100 Å, with further deposition resulting in an increase in island size. However, the island sizes remain constant as the Pd coverage increases beyond 0.4 ML, and new, smaller islands are formed in the areas between the larger islands and also closer to the step edges. This indicates a reduction in the mobility of the Cu atoms as the Pd coverage increases, resulting in the nucleation of new islands, while at low coverages, the Pd density is insufficient to lower the mobility.

Fig. 4. A 200 × 200 Å² STM image following 0.55 ML Pd deposition. Domains of c(2 × 2) structures can be seen although there is a high density of defects (~13%). Note the lack of Pd features on the upper step edge in the center of the image.

3.2. *c(2 × 2) alloy structure*

In order to try to achieve a sufficient density of chains to create large, ordered domains of the c(2 × 2) phase, the Pd coverage was increased to 0.55 ML (RBS), as shown in Fig. 4. Although domains of c(2 × 2) are indeed observed, they show a high density of defects (13%). Corrugation heights within the c(2 × 2) structure are measured to be on the order of 0.15 Å, compared to the ~0.02 Å outward displacement of the Pd atoms obtained from LEED data [11], indicating that the origin of the corrugation is due to the electronic rather than the geometric structure of the surface. Furthermore, in the vicinity of the upper step edges, there is a significantly reduced concentration of Pd, which further substantiates the assumption that in addition to forming islands, the Cu atoms, ejected by the formation of the alloy, migrate to nearby step edges. It can be seen from Fig. 4 that the alloy on the lower terrace extends right up to the step edge, indicating that the step grows out over the c(2 × 2) phase and resulting in areas of c(2 × 2) being located subsurface at such sites. In addition, there do not appear to be any domain boundaries within the c(2 × 2) structure despite the initial random nucleation of the Cu–Pd rows, indicating that there is movement of the Pd chains as the c(2 × 2) structures are formed so as to remove domain walls, thus resulting in larger domains.

The observation of very Cu-rich regions close to upper step and island edges (Fig. 4) reveals the origin of the inhomogeneity in structure of the c(2 × 2) alloy, reported by Valden et al. [19] on the basis of thermal desorption spectroscopy (TDS). Using CO as a probe molecule, they found that at a Pd coverage of 0.55 ± 0.1 ML a significant fraction of the outermost layer was pure Cu.

Well ordered domains of c(2 × 2) structure were formed only by increasing the Pd coverage significantly beyond 0.55 ML. Images taken following 1.1 ML deposition, as shown in Fig. 5a, reveal that the steps and islands have begun to merge, with higher resolution images (Fig. 5b), showing the nucleation of the second-layer structure at upper step and island edges; it is only away from these areas that the well ordered c(2 × 2) phase is observed, as shown in Fig. 5c with an atomic model

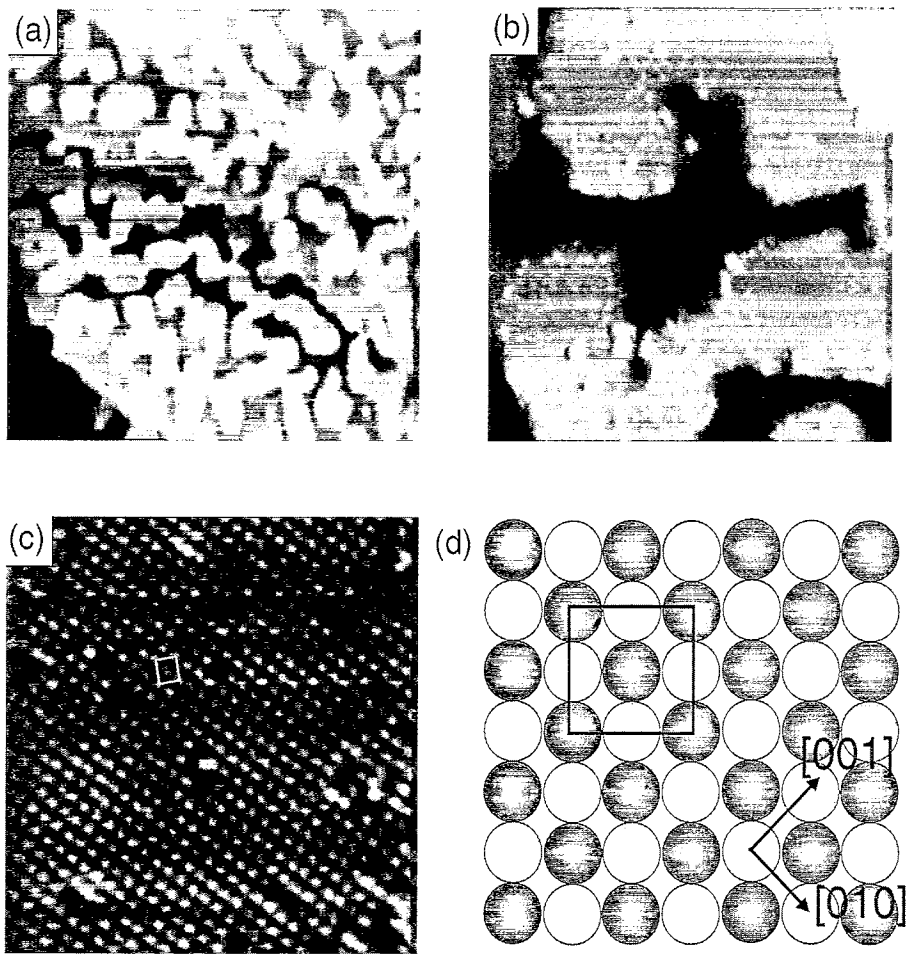

Fig. 5. (a) A 1500×1500 Å^2 image following 1.10 ML Pd deposition, showing the merging of islands and steps. (b) 300×300 Å^2 image showing the nucleation of a second-layer structure at upper step edges. (c) 100×100 Å^2 image recorded away from the step edges, showing well ordered c(2 × 2) structures. (d) Schematic model of the c(2 × 2) alloy structure. Pd (Cu) atoms heavily (lightly) shaded circles.

depicted in Fig. 5d. No distortion of the c(2 × 2) structure due to strain induced by the 8% size mismatch between Pd and Cu was seen in the images, unlike for the c(2 × 2) alloy structure formed by Au deposition on Cu(100), in which ridges are seen (mismatch 13%) [7]. Somewhat surprisingly, and in contrast to the case for Pd alloying, there is no subsurface Au in the Au/Cu(100) case, despite the fact that Cu and Au form bulk alloys.

The results presented here also shed light on the reason for the reported variations in Pd coverage necessary to form the c(2 × 2) alloy. Previously, this has mainly been determined as the coverage giving the maximum intensity of fractional order spots in the LEED pattern. However, although well ordered domains are observed away from the step/island edges at these coverages, the LEED pattern is obtained from a much wider area, and will consequently be affected to some extent by the disorder caused to the c(2 × 2) structure by growth of the second layer which nucleates before the c(2 × 2) structure is complete. If, on the other hand, the coverage is below the point where second layer nucleation occurs, then the disorder within the c(2 × 2) phase itself increases (Fig. 4), and in areas close to upper step and island edges, there are hardly any ordered Pd features. Thus the two types

of disorder will be present over a range of coverages, making it difficult to determine an optimum coverage for a well ordered $c(2\times2)$ structure.

3.3. Second-layer growth: $p(2\times2)p4g$ structure

Higher-resolution images of the structures formed by second-layer nucleation in the vicinity of upper step and island edges are shown in Fig. 6. The features, which protrude approximately 0.5 Å relative to the $c(2\times2)$ alloy level, are aligned along the [011] and [0$\bar{1}$1] directions with a spacing of 5.1 Å and thus form small domains with a $p(2\times2)$ periodicity. Fig. 5 and Fig. 6 confirm that the initial second-layer growth occurs preferentially close to upper step and island edges, that is, in areas where there is an excess of Cu atoms, due to the accumulation of Cu ejected from the terraces during the formation of the $c(2\times2)$ structure. Since the regions, in which the second layer nucleates, cover areas of the $c(2\times2)$ phase (see also Fig. 4), these observations confirm the proposal that the $c(2\times2)$ structure acts as a template for second-layer growth [20,22].

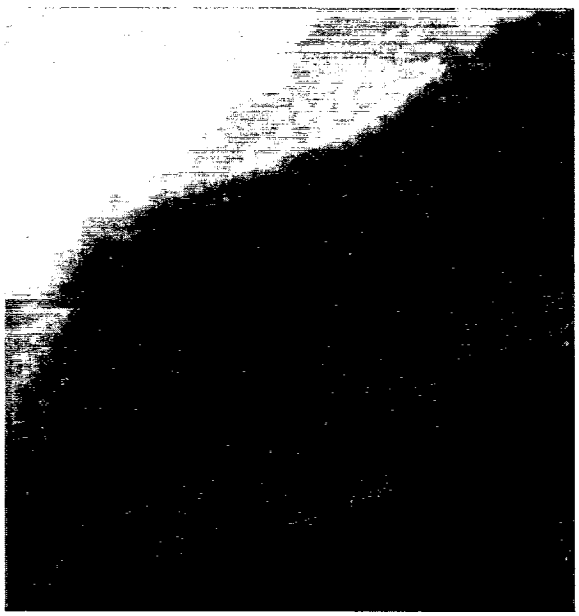

Fig. 6. A 200×200 Å^2 image showing the nucleation of a second layer structure, occurring on the upper edges of steps and islands. Where the features are ordered, they have a $p(2\times2)$ periodicity.

Increasing the coverage to 1.3 ML (RBS) results in the terraces and islands becoming covered by such features. Large-scale images, Fig. 7a, show an abundance of small islands covered by the second-layer structures that were observed at the upper step edges of Fig. 6. From the MEIS/LEIS studies [20,22] it is known that the topmost layer is a mixed Pd/Cu structure. This implies that Cu must be transported to the surface from underlying layers. It can be seen that the islands at this coverage are somewhat smaller and broken up

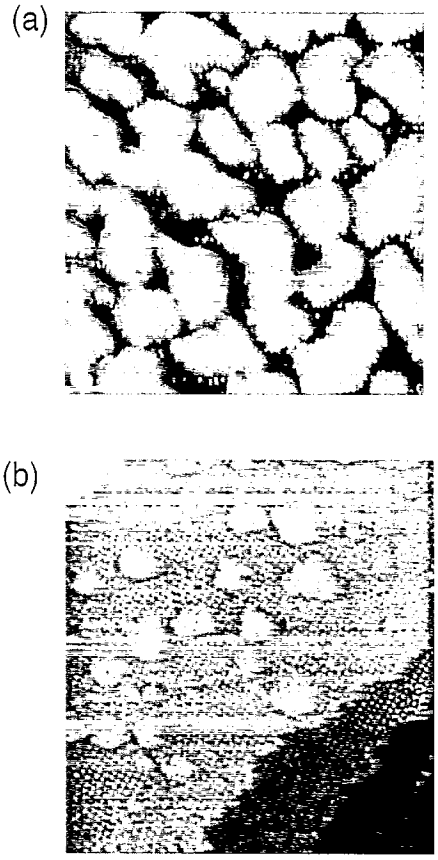

Fig. 7. (a) 500×500 Å^2 image following deposition of 1.3 ML of Pd. The terraces can be seen to consist of a large number of islands formed by the initial growth of the $c(2\times2)$ structure. Upon the islands, second-layer structures consistent with those seen on the upper step/island edges of Fig. 6 are observed. (b) 300×300 Å^2 image corresponding to 1.3 ML following annealing to 350 K in which the troughs/pits seen in (a) have been annealed out, creating smoother terraces on which the second layer structure is seen. The structure has $p(2\times2)$ periodicity, as determined from STM, and a large number of domain boundaries can be observed.

compared to Fig. 5, where the nucleation of the second layer has only just begun. Such a break-up may be indicative of a mechanism by which Cu is transported to the top layer, and which may involve an exchange with Pd atoms. An exact mechanism is difficult to propose from the STM data as we are unable to follow the nucleation of the second-layer structure in real time, and instead can only take snapshots at certain points in the growth process. However, the growth process does not appear to be kinetically limited at RT by Cu transport to the surface layer.

This is further supported by results from slightly annealing the sample to 350 K following deposition. The only change is that the surface morphology is much smoother, as shown in Fig. 7b, and consequently easier to image, but with the same $p(2\times2)$ structures as observed on the islands imaged in Fig. 7a. This is consistent with an observed sharpening of the LEED pattern upon annealing the second-layer structure, as reported by Pope et al. [20]. It can also be seen that in contrast to the $c(2\times2)$ alloy, the second-layer structure contains many domain boundaries.

More information on the structure can be obtained from high-resolution images, as shown in Fig. 8. In the center of the four atoms forming the $p(2\times2)$ structure, a smaller feature is observed, imaged approximately 0.2 Å lower. Given that the MEIS/LEIS data evidence Cu in the top layer [20,22], we propose that these features are Cu atoms. This is also consistent with the initial nucleation at upper step/island edges, which have an abundance of Cu, and the roughening of the terraces by island/trough formation. In addition, during the initial stages of the $c(2\times2)$ alloy formation, the Pd atoms are normally observed as being higher than the Cu atoms (cf. Fig. 2a).

In contrast to the simple $p(2\times2)$ periodicity imaged with STM, LEED studies have evidenced a $p(2\times2)$p4g structure [13,20–22]. Previous studies have attempted to address this structure, which has proven to be much more complex than p4g "clock" structures induced on Ni(100) by C and N [27–29]. Pope et al. [20] attempted fitting various models to their MEIS and LEED data. Following LEED analysis, the best fit to the data was a combination of a close-packed Pd layer

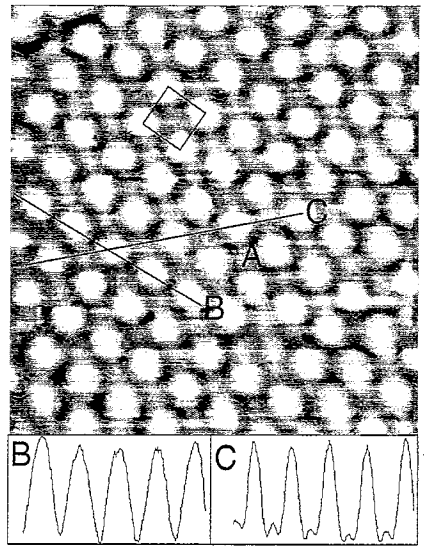

Fig. 8. High-resolution (50×50 Å^2) image of the second-layer structure. No evidence of a p4g structure can be seen in the surface layer. In the center of the $p(2\times2)$ structure, a smaller feature can be resolved (labeled A). Line profiles taken along the lines B and C are shown below the image with C showing the protrusions in the center of the $p(2\times2)$ structure. The height corrugations are 0.5 and 0.4 Å respectively.

above the $c(2\times2)$ alloy structure, with the Pd atoms in the top layer rotated in the clock fashion [27], and the remaining 20% part of the surface consisting of just the $c(2\times2)$ alloy. In addition, embedded atom method (EAM) calculations were performed, which confirmed that the Pd atoms on the $c(2\times2)$ structure would be stable. However, none of the simple p4g models proposed could fit completely with the MEIS data. In a LEIS study by Yao et al. [22] models were also proposed, in which a randomly mixed and clock-rotated Pd/Cu layer was located on top of the $c(2\times2)$ structure.

A number of comparisons can be made between the STM images recorded on the second-layer structure and the previously proposed models which were based on the p4g symmetry of the LEED patterns. Such p4g structures have been imaged successfully by STM on several systems [28–30], but in the present case, only features that have a $p(2\times2)$ periodicity are observed. Hence, from symmetry arguments, the models discussed above cannot be correct. The models proposed by Pope et al. have inhomogeneous regions consisting of (100) Pd layers and mixed Pd/Cu areas, with

the p4g symmetry arising from the Pd regions [20]. These models are at variance with the STM data which clearly show that the structure of the topmost layer is not inhomogeneous, the p(2 × 2) phase extending across the entire surface. Hence the origin of the p4g symmetry must be different from a rotated, (100) Pd top layer. Furthermore, the (100) structures would require an additional 1 ML Pd for the second layer. However, RBS measurements for a fully developed second-layer structure reveal that the coverage is on the order of 1.3 ML. As was shown earlier, on the order of 1.1 ML Pd is necessary to initiate the second-layer growth and complete the c(2 × 2) structure due to subsurface Pd. Thus, if the topmost layer consisted of close-packed Pd structures, a total coverage on the order of 2 ML would be required.

Although the STM results presented here do not give evidence for a definitive structural model, we have attempted to propose a model, as shown in Fig. 9, which is consistent with both the STM results and previous ion-scattering studies. Given that no rotation of the surface atoms is observed in the top layer of the structure by STM, we propose a model in which the underlying c(2 × 2) alloy layer is rotated in a clock mechanism instead. Such a restructuring would also lead to an expansion of fourfold hollow sites to accommodate the larger Pd atoms. In addition, the top layer is a mixed Pd/Cu layer with 50% Pd and 50% Cu consistent with the STM observation of a p(2 × 2) periodicity. This is also supported by LEIS results of Yao et al. [22] which showed a composition in the topmost layer of approximately 50% Cu and Pd. The incorporation of Cu in the topmost layer is further evidenced by pit formation together with initial nucleation at Cu rich upper steps. Taking into account the subsurface Pd, the Pd coverage required to form this model closely matches that measured by both this and previous studies for this structure.

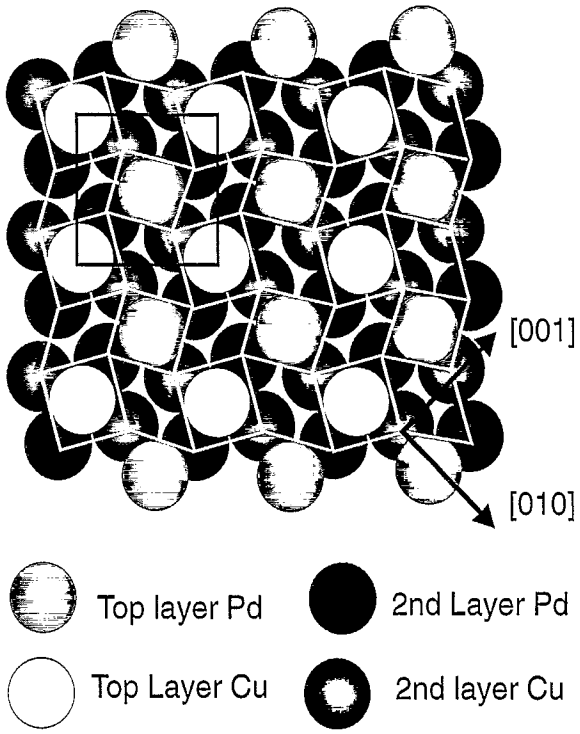

Fig. 9. Proposed model for the (2 × 2)p4g structure based on the STM results presented and previous ion scattering studies [19,21]. This consists of two mixed Cu/Pd layers. The surface layer is composed of a p(2 × 2) structure, consisting of 0.25 ML Pd and Cu, which is located on top of the "clock rotated" c(2 × 2) alloy phase. The (2 × 2) unit cell is marked together with the p4g symmetry of the lower layer.

4. Summary

In summary, we have used STM to study the growth and structure of Pd alloys on Cu(100) from initial nucleation up to second layer growth. Atomic-resolution images have shown that initial growth proceeds via the formation of chains of Pd atoms alloyed into the surface along the [010] and [001] directions, with the Pd atoms preferentially occupying second NN positions. Islands of Cu formed by the ejected Cu atoms are also observed, and as the coverage increases, the mobility of the Cu atoms is lowered, manifested by the nucleation of new islands in areas between existing ones. Also the islands are observed to nucleate on top of alloyed areas, resulting in subsurface Pd. The c(2 × 2) structure develops as the chains converge, although the long-range order of the c(2 × 2) structure is determined by an interplay between defects within the c(2 × 2) at lower coverages and the initiation of second layer growth at increased coverages before the c(2 × 2) is fully completed. This provides an explanation for the reported

discrepancy in the coverage required to form a well ordered c(2 × 2) structure.

A second layer is observed to nucleate at upper step and island edges on top of underlying areas of a c(2 × 2) alloy. The second-layer growth continues with further deposition, and although LEED shows a p4g symmetry for this phase, STM images reveal that the top layer has a simple p(2 × 2) structure. Based on the STM results and previous studies, we have proposed a model for this structure which consists of a p(2 × 2) top layer, comprised of one Pd and one Cu atom per unit cell, located on top of a clock-rotated c(2 × 2) structure.

Acknowledgements

We would like to acknowledge financial support from the "Center for Atomic-scale Materials Physics" (CAMP), sponsored by the Danish National Research Foundation, an EU network on "Bond Making and Breaking at Surfaces" and the Danish Science Research Councils via the "Center for Surface Reactivity".

References

[1] E. Bauer, Z. Krist. 110 (1958) 372.
[2] U. Bardi, Rep. Prog. Phys. 57 (1994) 939.
[3] L. Pleth Nielsen, F. Besenbacher, I. Stensgaard and E. Lægsgaard, Phys. Rev. Lett. 71 (1993) 754.
[4] H. Röder, R. Schuster, H. Brune and K. Kern, Phys. Rev. Lett. 71 (1993) 2086.
[5] P. Hu, A. Wander, L.M. Delagarza, M.P. Bessent and D.A. King, Surf. Sci. 293 (1993) L917.
[6] C. Nagl, E. Platzgummer, O. Haller, M. Schmid and P. Varga, Surf. Sci. 331–333 (1995) 831.
[7] D.D. Chambliss and S. Chiang, Surf. Sci. 264 (1992) L187.
[8] M. Wuttig, Y. Gauthier and S. Blügel, Phys. Rev. Lett. 70 (1993) 3619.
[9] H.P. Noh, T. Hashizume, D. Jeon, Y. Kuk, H.W. Pickering and T. Sakurai, Phys. Rev. B 50 (1994) 2735.
[10] R.G.P. van der Kraan and H. van Kempen, Surf. Sci. 338 (1995) 19.
[11] S.C. Wu, S.H. Lu, Z.Q. Wang, C.K.C. Lok, J. Quinn, Y.S. Li, D. Tian, F. Jona and P.M. Marcus, Phys. Rev. B 38 (1988) 5363.
[12] G.W. Graham, P.J. Schmitz and P.A. Thiel, Phys. Rev. B 41 (1990) 3353.
[13] T.D. Pope, K. Griffiths and P.R. Norton, Surf. Sci. 306 (1994) 294.
[14] T.D. Pope, G.W. Anderson, K. Griffiths, P.R. Norton and G.W. Graham, Phys. Rev. B 44 (1991) 11518.
[15] V. Ponec, Surf. Sci. 272 (1992) 111.
[16] S. Leviness, V. Nair, A.H. Weiss, Z. Schay and L. Guczi, J. Molecular Catalysis 25 (1984) 131.
[17] G.W. Graham, Surf. Sci. 171 (1986) L432.
[18] J. Kudrnovský, S.K. Bose and V. Drchal, Phys. Rev. Lett. 69 (1992) 308.
[19] M. Valden, J. Aaltonen, M. Pessa, M. Gleeson and C.J. Barnes, Chem. Phys. Lett. 228 (1994) 519.
[20] T.D. Pope, M. Vos, H.T. Tang, K. Griffiths, I.V. Mitchell, P.R. Norton, W. Liu, Y.S. Li, K.A.R. Mitchell, Z.-J. Tian and J.E. Black, Surf. Sci. 337 (1995) 79.
[21] J. Yao, Y.G. Shen, D.J. O'Connor and B.V. King, J. Vac. Sci. Technol. A 13 (1995) 1443.
[22] J. Yao, Y.G. Shen, D.J. O'Connor and B.V. King, unpublished.
[23] P.W. Murray, I. Stensgaard, E. Lægsgaard and F. Besenbacher, Phys. Rev. B 52 (1995) R14 404.
[24] L. Eierdal, F. Besenbacher, E. Lægsgaard and I. Stensgaard, Surf. Sci. 312 (1994) 31.
[25] I. Stensgaard, Rep. Prog. Phys. 55 (1992) 989.
[26] J. Tersoff, Phys. Rev. Lett. 74 (1995) 424.
[27] J.H. Onuferko, D.P. Woodruff and B.W. Holland, Surf. Sci. 87 (1979) 357.
[28] C. Klink, L. Olesen, F. Besenbacher, I. Stensgaard, E. Lægsgaard and N.D. Lang, Phys. Rev. Lett. 71 (1993) 4350.
[29] F.M. Leibsle, Surf. Sci. 297 (1993) 98.
[30] C. Klink, I. Stensgaard, F. Besenbacher and E. Lægsgaard, Surf. Sci. 342 (1995) 250.